A Precise Approach Calibrated by Experimental Data to Make an Artificial Impulse

Toshiko Iguchi, Tetsuya Kodama and Hiroshi Noborio

Division of Information and Computer Science
Graduate School of Engineering
Osaka Electro Communication University
Hatsu-Cho 18-8, Neyagawa 572-8530, Japan

Abstract

Baraff's and Mirtich's approaches are well known so as to generate force and impulsive force artificially at collision between rigid bodies. However, both cannot be unfortunately applied for a practical use such as complex dynamic animation and simple haptic rendering. The reason is as follows: Baraff's approach deals with many forces at multiple contacts, but does not always calculate a solution under static and dynamic frictions. Moreover, since almost natural contact phenomena should be operated by not force but impulse (a sequence of forces) supervised by time, his approach cannot manage such practical aspects. On the other hand, Mirtich's approach completely neglects time, e.g., the interval of collision, and consequently make only an impulsive force (does not generate a true impulse as force distribution). Consequently, they cannot be applicable to dynamic animation including simultaneous multiple contacts and haptic rendering. For this reason, we propose a new approach based upon integration of an arbitrarily chosen force distribution over a finite time interval by time. Also, we discuss a new method to calibrate completely the force distribution and uncertain parameters required in our new approach. By the deep calibration, the accuracy of linear tangential and angular impulses in our approach is superior to that of these impulsive forces in Mirtich's approach.

1. Introduction

The physical-based approach, e.g., contact force/impulsive force calculation, has been focused in the last decade for many applications such as dynamic animation and haptic control. This theoretical area was revisited by Baraff [1,2], and then have been aggressively studied by many researchers as Mirtich, Kawachi and so on [3,4,5,6,7].

Baraff presented a simple and fast algorithm for calculating forces at multiple contacts between rigid bodies by formulating relationship between forces and relative accelerations as LCP (Linear Complementarily Problem) [2]. The algorithm is based on Dantzig's algorithm for solving LCP. However, his approach does not always get a solution under not only static friction but also dynamic friction. In succession, Mirtich presented a smart algorithm for calculating an impulsive force independing time [3,4,5]. His assumption is that an impulse is generally a very large force occurring over a very small time and that it is most of the time considered as infinitesimal. Therefore, his approach does not generate a real impulse (force distribution) controlled by time. Consequently in his approach, we cannot feel any artificial impulse by a haptic device, and we cannot generate complex dynamic animation including simultaneous multiple contacts. Also, Mirtich's approach calculates linear tangential and angular impulsive forces from a vertical impulsive force without considering what happen during collision deeply. Especially, Coulomb's static and dynamic friction laws are unfortunately confused for determining whether encountered bodies are sticking or sliding each other. For this reason, linear tangential and angular impulsive forces made in his approach are not accurate. Finally, Kawachi mixed Baraff's force approach with multiple contacts and Mirtich's impulsive force approach with the unique contact in his 2-D and 3-D approaches [6,7]. He straightforwardly mixed Mirtich's and Baraff's approaches without eliminating their disadvantages. Consequently, his approach still keeps their drawbacks. As a result, we cannot feel any impulse (a sequence of forces) by haptic, and also we cannot generate any dynamic animation whose linear and angular velocities of bodies after each

collision are correct against a real world in such famous approaches.

To overcome their problems, we firstly adopt a more general definition of **impulse**, which is the integral of a force over a finite time interval in this paper. In this more general sense, our impulse extremely differs from **impulsive force** frequently referred in the CG community as impulse. Secondly, we propose a new approach to compute linear tangential and angular impulses from a linear vertical impulse artificially chosen as force distribution based on time, namely Gaussian. The new approach consists of Newton's force equation, Euler's moment equation, Coulomb's static friction inequality and dynamic friction equation in order to exchange force and moment between bodies during collision. Furthermore, various parameters can be estimated thanks to an experimental setup. In order to calibrate a linear vertical impulse, parameters of our new approach, i.e., dynamic friction coefficient μ_d, the maximum coefficient of static friction μ_s, reflection coefficient E between encountered bodies in many different aspects, we measure many force/moment distributions between bodies by 6-degrees-of-freedom (DOF) force/moment sensor during collision, whose sampling time is 125 [μs], we measure many linear/angular acceleration sequences of a 2-D body by two acceleration scales during collision, whose sampling time is 20 [μs], and we measure many linear/angular velocities before and after collision by the high-speed camera, whose sampling time is 1 [ms].

The paper is organized as follows: Section 2 describes our physical-based approach based on Newton's force equation, Euler's moment equation, and Coulomb's dynamic friction equation and static friction inequality. They run during collision to exchange force and moment between encountered bodies. The quadratic differential equations are approximately solved by the fourth-ordered Runge-Kutta method. In section 3, we explain how to design a linear vertical impulse and also how to calibrate the impulse and unknown parameters in our approach so as to make linear tangential and angular impulses. If encountered bodies are affected by precise linear/angular impulses (linear/angular momentum variations), their linear/angular velocities after collision can be exactly generated from those before collision in dynamic animation. Also, practical force distribution can be felt by a human operator via some haptic during collision. In section 4, we will give some experimental works to identify internal force/moment of a body used in Newton's force and Euler's moment equations from its linear/angular velocities. Then in section 5, we compare linear/angular velocities after collision, which are made in a real experiment, Mirtich's classic approach, and our new approach. As a result, we ascertain that our new approach is always better than Mirtich's one for several contact trials. Finally in section 6, we present a few concluding remarks and future extensions.

2. Our New Impulse-Based Approach

Mirtich's approach is an approximated approach to calculate linear tangential impulsive forces from a linear vertical one, which are distinguished by the contact surface between two encountered bodies. First of all, since X, Y and Z components p_x, p_y and p_z of an assumed impulse **p** are differentiated by Z component p_z, we cannot deal with time, *e.g.*, time interval during collision. Moreover, because of the differentiation, vertical force p'_z is always fixed as one and consequently its accumulated impulsive force p_z increases linearly (Fig.1(a)). Also, since linear tangential forces p'_x and p'_y are dynamic frictions of p'_z along X and Y-axes, their integrated impulsive forces p_x and p_y exactly or approximately increase linearly. It depends on dimension, shape and material of bodies. For this reason, we cannot obtain any impulse p_x, p_y or p_z as force distributions. Furthermore, Mirtich does not regard any internal force of a body during collision at all. He regards only a given external force p'_z and its calculated external friction forces p'_x and p'_y. These are defective points to calculate practical impulses (force distributions) precisely.

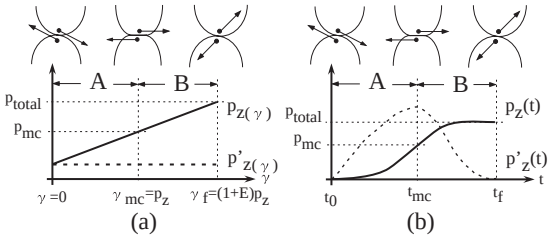

Figure 1: *Compression phase* **A** *and restitution phase* **B** *between two bodies during collision (a) in Mirtich's classic approach and (b) in our new approach.*

To overcome such problems, we propose a new approach. The differences against Mirtich's approach are sequentially described as follows:

1. Each external force $p'_z(t)$ is sequentially given in an artificial impulse (force distribution) $p_z(t)$ in time as illustrated in Fig.1(b). The artificial impulse $p_z(t)$ is precisely calibrated from real distributions measured by 6 DOF force/moment sensor

2. A set of internal force/moment of a body before collision is determined by a set of linear/angular velocities of the body before collision.

3. Coulomb's static friction inequality under present internal forces and moments of encountered bodies judges whether they are sliding or sticking.

4. If and only if two bodies are sliding, **Coulomb's dynamic friction equation** calculates their dynamic friction forces as tangential external forces $p'_x(t)$ and $p'_y(t)$. Otherwise, no dynamic friction force exists, i.e., $p'_x(t) = p'_y(t) = 0$. Then in **Newton's force equation**, $p'_x(t)$, $p'_y(t)$ and $p'_z(t)$ are added into present internal forces. Synchronously in **Euler's moment equation**, external moments are added into present internal moments.

5. By integrating all the external forces $p'_x(t)$, $p'_y(t)$ and $p'_z(t)$, we finally obtain three linear impulses $p_x(t)$, $p_y(t)$ and $p_z(t)$ and also three angular impulses.

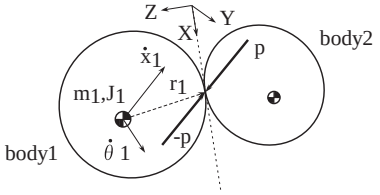

Figure 2: *Collision between two bodies.*

m_i : mass of an object (i : body number)
$\dot{\mathbf{x}}_i$: linear velocity of an object
$\dot{\theta}_i$: angular velocity of an object
$\mathbf{r}_i$: contact point relative to c.o.m.
$\mathbf{J}_i$: mass matrix
$\mathbf{p}$: impulse encountered by body 2 on body 1
$\mathbf{u}_i$: relative linear velocity of contact point
$\mathbf{u}_{\theta_i}$: relative angular velocity of contact point
$\dot{\mathbf{x}}_b = [\dot{x}_{bx}, \dot{x}_{by}, \dot{x}_{bz}]^T$: linear velocity before collision
$\dot{\mathbf{x}}_a = [\dot{x}_{ax}, \dot{x}_{ay}, \dot{x}_{az}]^T$: linear velocity after collision
$\dot{\theta}_b = [\dot{\theta}_{bx}, \dot{\theta}_{by}, \dot{\theta}_{bz}]^T$: angular velocity before collision
$\dot{\theta}_a = [\dot{\theta}_{ax}, \dot{\theta}_{ay}, \dot{\theta}_{az}]^T$: angular velocity after collision

The linear velocity variation at a contact point of body i during collision is calculated by linear and angular relative velocity variations of encountered bodies. This relationship is expressed in the equation (1) under Newton-Euler equations. Consequently as shown in the equation (2), the linear velocity variation at the contact point is converted from a vertical impulse via the matrix $\mathbf{M}_i$.

$$\Delta\mathbf{u}_i(t) = \mathbf{u}_i(t) - \mathbf{u}_i(0) = \Delta\dot{\mathbf{x}}_i(t) + \Delta\dot{\theta}_i(t) \times \mathbf{r}_i. \quad (1)$$

$$\Delta\mathbf{u}_i(t) = [\frac{1}{m_i}\mathbf{I} - \tilde{\mathbf{r}}_i\mathbf{J}_i^{-1}\tilde{\mathbf{r}}_i]\mathbf{p}(t) = \mathbf{M}_i\mathbf{p}(t). \quad (2)$$

$\mathbf{I}$ is the 3×3 identity matrix, $\tilde{\mathbf{r}}_i$ is the canonical 3×3 skew-symmetric matrix corresponding to $\mathbf{r}_i$, and $\mathbf{M}_i$ is the 3×3 matrix dependent only upon the masses and mass matrices (inertia tensor) of colliding bodies, and the location of contact point relative to the mass center.

The angular velocity variation at a contact point of body i during collision is calculated by only the angular relative velocity variation of encountered bodies. This relationship is expressed in the equation (3) under Euler's equation. Consequently as shown in the equation (4), the angular velocity variation at the contact point is converted from a vertical impulse via the matrix $\mathbf{M}_{\theta i}$.

$$\Delta\mathbf{u}_{\theta i}(t) = \mathbf{u}_{\theta i}(t) - \mathbf{u}_{\theta i}(0) = \Delta\dot{\theta}_i(t). \quad (3)$$

$$\Delta\mathbf{u}_{\theta i}(t) = [\mathbf{J}_i^{-1}\tilde{\mathbf{r}}_i]\mathbf{p}(t) = \mathbf{M}_{\theta i}\mathbf{p}(t). \quad (4)$$

Two kinds of matrices $\mathbf{M}_i$ and $\mathbf{M}_{\theta i}$ are only depending on dimension, shape and material, and therefore they are constant during collision. By mixing the matrices $\mathbf{M}_i$ and $\mathbf{M}_{\theta i}$, we can get $\mathbf{M}$ and equation (5).

$$\Delta\mathbf{u}(t) = \mathbf{M}\mathbf{p}(t). \quad (5)$$

Since $\mathbf{M}$ is constant over the entire collision, we can differentiate equation (5) with respect to time t to obtain

$$\mathbf{u}'(t) = \mathbf{M}\mathbf{p}'(t). \quad (6)$$

Moreover, we always process internal forces/moments of encountered bodies in the Coulomb's static friction inequality and dynamic friction equation. In general, the bodies are sliding or sticking during collision. First of all, we consider the **law of action and reaction**. An internal force of a body is to be the action force of its encountered body, and consequently the former body is received by the same reaction force from the latter body. For each body, a vertical reaction force equals to its vertical internal force, whose directions are opposite. The vertical reaction force leads a friction force, whose direction are opposite to a tangential action force. For this reason, the switching between sliding and sticking modes are determined by the balance of a tangential action force and a friction force made from a vertical action force. The vertical and tangential internal forces $\mathbf{F}(t) = [F_x(t), F_y(t), F_z(t)]^T$ and moment $\mathbf{N}(t) = [N_x(t), N_y(t), N_z(t)]^T$ are distinguished by the contact surface of encountered bodies. Here, the balance of tangential action and friction forces is calculated in Coulomb's static friction inequality. The maximum of static friction coefficient is denoted as μ_s.

$$|\sqrt{F_x(t)^2 + F_y(t)^2}| \leq \mu_s|F_z(t)\ |. \quad (7)$$

Note that calculation of the initial internal force $\mathbf{F}(0)$ and moment $\mathbf{N}(0)$ before collision is described in the section 4.

Furthermore, we always consider internal moment of the body in the above balance. $\mathbf{F_N}(t) = [F_{Nx}(t), F_{Ny}(t), F_{Nz}(t)]^T$ is the force converted from the moment $\mathbf{N}(t) = [N_x(t), N_y(t), N_z(t)]^T$ by $\mathbf{N}(t) = \mathbf{r}\times\mathbf{F_N}(t), \quad \mathbf{r} = [r_x, r_y, r_z]^T$. Especially in case of 2-D coordinate system, we give $r_x = r_y = 0$ and $F_y(t) = 0$. Therefore,

$$F_{Nz}(t) = F_{Ny}(t) = 0, \ \ F_{Nx}(t) = N_y(t)/r_z$$

If we add this affection into the equation (7), we obtain the following equation concerning to static friction.

$$|\sqrt{(F_x(t) + F_{Nx}(t))^2 + (F_y(t))^2}| \leq \mu_s|F_z(t)\ |. \quad (8)$$

This inequality is satisfied, we move to the *Sticking Mode* (STM), otherwise, we move to the *Sliding Mode* (SLM).

Sliding mode (SLM) If the inequality (8) is not maintained, a relative velocity $u_x(t) \neq 0$ or $u_y(t) \neq 0$ is obtained. In this case, tangential component $p'_x(t)$ or $p'_y(t)$ and normal component $p'_z(t)$ completely appear. Three components $p_x(t)$, $p_y(t)$ and $p_z(t)$ of impulse are calculated by integrating $p'_x(t)$, $p'_y(t)$ and $p'_z(t)$ during collision. The tangential external forces $p'_x(t)$ and $p'_y(t)$ are always calculated from a vertical external force $p'_z(t)$ of a given impulse $p_z(t)$ by the Coulomb's dynamic friction equation. The dynamic friction coefficient is denoted as μ_d.

$$\begin{bmatrix} u'_x(t) \\ u'_y(t) \\ u'_z(t) \end{bmatrix} = \mathbf{M} \begin{bmatrix} -\mu_d \frac{u_x(t)}{\sqrt{{u_x}^2(t)+{u_y}^2(t)}} \cdot p'_z(t) \\ -\mu_d \frac{u_y(t)}{\sqrt{{u_x}^2(t)+{u_y}^2(t)}} \cdot p'_z(t) \\ p'_z(t) \end{bmatrix}. \quad (9)$$

The integration is done by the fourth-order Runge-Kutta

method. The sampling time for integrating force components $p'_x(t)$, $p'_y(t)$, $p'_z(t)$ and their moments is the same against the sampling time, i.e., 20 [μs] of two acceleration scales to determine internal force/moment components.

Sticking mode (STM) If the inequality (8) is kept, relative velocities are set as zero, i.e., $u_x(t) = 0$ and $u_y(t) = 0$. In this case, because of (9), tangential components $p'_x(t)$ and $p'_y(t)$ disappear. Therefore, only the normal component $p'_z(t)$ is integrated for calculating an artificial impulse $p_z(t)$.

The internal force/moment is always renewed by the external force $\mathbf{p}'(t) = [p'_x(t), p'_y(t), p'_z(t)]^T$ and moment. As a result, the internal force $\mathbf{F}(t) = [F_x(t), F_y(t), F_z(t)]^T$ and moment $\mathbf{N}(t) = [N_x(t), N_y(t), N_z(t)]^T$ are always revised during collision per the sampling time 20 [μs] as follows:

$$\mathbf{F}(t+1) = \mathbf{F}(t) + \mathbf{p}'(t), \quad \mathbf{N}(t+1) = \mathbf{N}(t) + \mathbf{r} \times \mathbf{p}'(t). \quad (10)$$

3. Construction of Vertical Artificial Impulse

In general, an arbitrary impulse can be represented as a normal distribution described in Fig.1(b). Therefore, we firstly measure many real impulses by 6 DOF force/moment sensor to investigate its shape including time interval and height. Consequently, the real impulse can be formulated by Gaussian. For this reason, we consider how to generate its approximated artificial impulse by Gaussian.

3.1. Initializing Uncertain Paremeters E, μ_s and μ_d

In our approach, reflection coefficient E between two bodies is used for generating an artificial impulse whose direction is vertical to the contact surface between encountered bodies. Then using two friction coefficients μ_s and μ_d, we calculate artificial impulses whose directions are tangential to the given vertical impulse. These parameters are invariable as long as dimension, material and shape of encountered bodies are the same.

The initial values of coefficients μ_d and μ_s are detected by the following simple experiments. Namely, an initial μ_d is calculated by $\mu_d = F_t/F_n$. F_t and F_n are magnitudes of tangential and normal forces on the contact surface of encountered bodies during sliding. F_t and F_n are directly measured by two spring balances. In addition, an initial μ_s is calculated by $\mu_s = F_{tmax}/F_n$. F_{tmax} is measured as the maximum magnitude of tangential force when two encountered bodies start to move on the contact surface. In general, the sliding is more stable than the switching. For this reason, we suppose the initial value of μ_d is more precise than that of μ_s. Thus, we calibrate μ_s and μ_d in this order.

Secondly, a lot of experimental pairs of normal components of linear velocities ($\dot{x}_{az}$ and $\dot{x}_{bz}$) before and after collision can be precisely measured by the high speed camera. Therefore, reflection coefficient $E = -\dot{x}_{az}/\dot{x}_{bz}$ between two bodies is independently calibrated as 0.523 by the least square method minimizing the value $(\dot{x}_{az} + E\dot{x}_{bz})^2$ under a lot of experimental pairs.

3.2. Analysis of an Impulse (Force Distribution) Measured by 6 DOF Force/Moment Sensor

In order to identify shape (interval, height, and so on) of many real impulses, we measure a lot of collisions between puck and wall by 6 DOF force/moment sensor (Fig.3 and 4). First of all, impulse area equals to momentum variation such as $p_z = m(\dot{x}_{az} - \dot{x}_{bz}) = -m(1+E)\dot{x}_{bz}$. For this reason, area of vertical impulse p_z is theoretically proportional to a vertical velocity $\dot{x}_{bz}$ before collision. This is experimentally ascertained (Fig.4(a)). Furthermore, the maximum force of vertical impulse p_z is experimentally proportional to a vertical velocity $\dot{x}_{bz}$ before collision (Fig.4(a)). Finally, as illustrated in Fig.4(b), we can experimentally understand collision intervals are the same in time.

On the observation, the height H of force distribution (the vertical maximum force p'_{zmax} of impulse) can be artificially created from a vertical velocity $\dot{x}_{bz}$ before collision. After gathering many pairs of maximum force p'_{zmax} and velocity $\dot{x}_{bz}$ before collision, we calibrate a constant value $s = p'_{zmax}/\dot{x}_{bz}$. Finally, we automatically calculate the height H as $H = s \cdot \dot{x}_{bz}$.

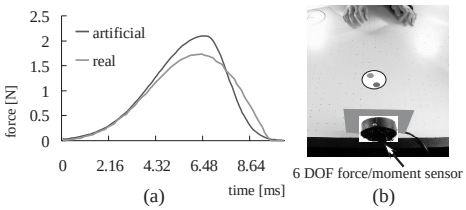

Figure 3: *(a) Artificial and real impulses (force distributions) between wall and puck. In case of a collision, the difference between areas of two impulses is evaluated as 0.003527 ∼ 0.000013 [kgm/s = N · s]. (b) Many collision impulses are measured by 6 DOF force/moment sensor.*

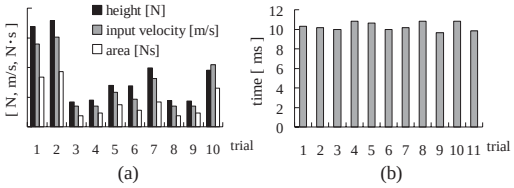

Figure 4: *Collision between wall and puck: (a) The proportional relation between height and input velocity and area of each impulse measured by the 6 DOF force/moment sensor. (b) Collision intervals are almost the same, which are measured by the 6 DOF force/moment sensor.*

Under these properties, we mention how to generate artificially vertical force distribution (impulse) p_z from a vertical velocity $\dot{x}_{bz}$ before collision. After recognizing reflection coefficient E, interval and height of impulse (force distribution), we combine different distributions as left and right parts of a vertical artificial impulse. The interval ratio of compression and restitution phases is theoretically defined as $1 : E$. The former is relatively gently-sloping and the latter is relatively steep slope.

As shown in Fig.3(a), left and right distributions are similar to the regular distribution. For this reason, we use the mixture equation (11) of Gauss's normal distribution and standard normal distribution. σ is the dispersion and α is the chance variable. H is already calculated as the height of force distribution.

$$p'_z(t) = He^{-\frac{(t-\alpha)^2}{2\sigma^2}} \quad (11)$$

If the height H is completely fixed in the mixture equation (11), the distribution interval is expanded as the distribution σ increases. For this reason, the smaller [larger] the parameter σ is, the larger [smaller] the slope of distribution is. From many kinds of experimental impulses, we can see that the slope in the compression phase **B** is larger than that in the restitution phase **A** as illustrated in Fig.1(b). For this reason, we keep the relationship $\sigma_A > \sigma_B$ to build an artificial impulse.

As illustrated in Fig.3(a), shape of an artificial impulse is similar to that of its real impulse. This similarity is useful to feel an artificial impulse by some haptic (Mirtich's approach cannot make any force distribution).

3.3. Calibration Method of an Artificial Impulse and Uncertain Parameters in Our Impulse-Based Approach

Until now, we design a linear vertical impulse p_z artificially, and then calculate linear tangential impulse p_x and angular impulse $p_{\theta y}$ artificially. In this paragraph, we propose a method to calibrate E, μ_s, μ_d and finally vertical impulse p_z (force distribution) by minimizing differences between artificially calculated linear and angular impulses p_z, p_x, p_{θ_y} and experimental linear momentum variations $m\Delta\dot{x}_z$, $m\Delta\dot{x}_x$, angular momentum variation $J\Delta\dot{\theta}_y$, respectively. In order to calculate $\Delta\dot{x}_z$, $\Delta\dot{x}_x$ and $\Delta\dot{\theta}_y$, we experimentally measure linear velocities $\dot{X}_{ax}$ and $\dot{X}_{az}$, angular velocity $\dot{\Theta}_{ay}$ after collision, and also linear velocities $\dot{X}_{bx}$ and $\dot{X}_{bz}$, angular velocity $\dot{\Theta}_{by}$ before collision.

In order to explain our calibration method, we give a collision example between two bodies illustrated in Fig.5.

Step 1 **Calibrating reflection coefficient E (Agreeing a calculated vertical impulse $p_z(t)$ with its experimental impulse):**
We coincide calculated vertical impulse $p_z(t)$ with its experimental real impulse by changing an initial E. The area of vertical impulse $p_z(t)$ can be controlled by reflection coefficient E, i.e., $p_z(t) = m\Delta\dot{x}_z = -m(1+E)\dot{x}_{bz}$. For this reason, E is precisely calibrated by area coincidence of virtual and real vertical impulses (Fig.5(a),(b)).

Step 2 **Calibrating static and dynamic friction coefficients μ_s and μ_d (Adjusting calculated tangential impulse $p_x(t)$):**
We calibrate μ_s and then μ_d because the former initial value is not always precise than the latter one. According to the equation (8), the larger the μ_s is, the larger the number of sticking mode is. In this case, the tangential impulse $p_x(t)$ decreases because each force $p'_x(t)$ is not integrated in the sticking mode (STM) (Fig.5(b),(c)). Moreover, according to the equation (9), the larger the μ_d is, the larger the tangential impulse $p_x(t)$. The reason is that each force $p'_x(t)$ integrated in the sliding mode (SLM) becomes larger (Fig.5(b),(c)). For this reason, μ_s and μ_d are precisely calibrated by the coincidence of areas of virtual and real tangential impulses.

Step 3 **Calibrating a calculated vertical impulse $p_z(t)$ (distribution of forces $p'_z(t)$):**
If we slightly change the vertical impulse in the Gaussian distribution initially given in the paragraph 3.2, we simultaneously adjust vertical and tangential impulses (Fig.5(c),(d)).

In such a scenario, we systematically and flexibly calibrate E, μ_s, μ_d and vertical impulse (force distribution) in this order.

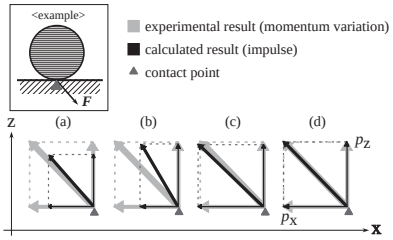

Figure 5: *(a) An initial state. (b) A state after calibrating reflection coefficient E (after adjusting the vertical impulse p_z independently). (c) A state after calibrating two kinds of friction coefficients μ_s and μ_d (after adjusting the tangential impulse p_x independently). (d) A state after calibrating force distribution of vertical impulse p_z (after calibrating vertical and tangential impulses simultaneously).*

As contrasted with this, we calibrate the area of vertical impulse (momentum variation) only by changing E, and calibrate the areas of tangential impulses only by changing μ_d in Mirtich's approach. His approach completely neglects to exchange force and moment between encountered bodies during collision, and also neglects to calibrate vertical impulse (force distribution) and static friction coefficient μ_s. For this reason, we cannot obtain any precise tangential impulsive force and impulsive moment.

4. Calculation of Initial Internal Force and Moment

First of all, we evaluate a sequence of accelerations measured by each acceleration scale. For this purpose, we locate two acceleration scales on a link of robotic manipulator. The manipulator equips precise encoders in two motors. Therefore, by calculating direct kinematics based on measured joint angles, we can obtain exact positions of scales on the link. On the other hand, by integrating accelerations of two scales from their initial positions, we independently capture positions of the scales. Finally, by comparing two positions measured by joint encoders and acceleration scales, we ascertain that a sequence of accelerations measured by each acceleration scale has high precision.

Secondly, we calculate linear and angular velocities of a puck measured by the two accelerations. In our experiment, we use puck, mallet, and wall whose materials are plastic. Therefore, we consider only a collision between objects with the same material. The weight, height and radius of puck are 8 [g], 2.0 [mm] and 32.4 [mm], respectively. Finally, we introduce correspondences between internal force/moment of

a puck and linear/angular velocities of the puck before collision. The equations are parameterized by the weight m and the radius r of a puck, and a sampling time Δt of integration from an impulse to its impulsive force.

4.1. Evaluation of Acceleration Precision Measured by the Acceleration Scales

In this paragraph, we experimentally evaluate acceleration precision of each scale. First of all, we allocate two acceleration scales on a link of the direct drive (DD) robot arm. By integrating their accelerations twice, we can calculate two positions located at the scales. Then we compare the positions with their corresponding ones measured under robot kinematics and motor angles.

In order to calculate a position of an acceleration scale (PCB Piezotronics Co.) in the real-time manner, we locate the scale on a robot link. First of all, each scale always captures X, Y, and Z accelerations at an arbitrary position in the sampling time 20 [μs]. By processing successive accelerations in a low-pass filter, we can remove their noises. Secondly, we integrate a sequence of accelerations two times so as to obtain a sequence of positions. In order to check the position accuracy, we use a direct-drive (DD) robot arm (Shinmeiwa Co.) illustrated in Fig.6(a).

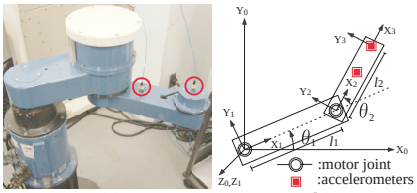

(a) (b)

Figure 6: *(a) A photo of DD arm with two acceleration scales described by circles. (b) A figure of robot kinematics with the scales.*

By setting two acceleration scales on a robot link shown in Fig.6(b), we measure sequences of their positions. In order to evaluate precision of each position, we compare that with its accurate position calculated by the direct kinematics, e.g., $x = l_1\cos(\theta_1) + l_2\cos(\theta_1+\theta_2), y = l_1\sin(\theta_1) + l_2\sin(\theta_1+\theta_2)$ based on motor angles acquired from joint encoders. The robot arm has two joints whose angles θ_1 and θ_2. The resolution is denoted as $360/2^{17}$ = 0.002747 [deg] (17bit). In this way, we can calculate X and Y coordinates of the acceleration scales located on the robot arm. In Fig.7(a),(b) we give X and Y coordinates measured from joint encoders and acceleration scales, respectively. The average errors are bounded by 1.311 [μm] along X axis and 0.987 [μm] along Y axis.

4.2. Linear/Angular Accelerations of a Puck Measured by Two Acceleration Scales

If a circular puck has linear acceleration $\ddot{x}$ and angular acceleration $\ddot{\theta}$, two acceleration scales $\ddot{x}_1$ and $\ddot{x}_2$ has linear accelerations $\ddot{x}_1 = \ddot{x} - \ddot{x}_{re}$ and $\ddot{x}_2 = \ddot{x} + \ddot{x}_{re}$. If the distance from the gravity center of puck to each acceleration scale is r, the acceleration of each scale is denoted by $\ddot{x}_{re} = \ddot{\theta} r$. Consequently, $\ddot{x}$ is calculated by $(\ddot{x}_1 + \ddot{x}_2)/2$ and also $\ddot{\theta}$ is calculated by $(\ddot{x}_1 - \ddot{x}_2)/2r$.

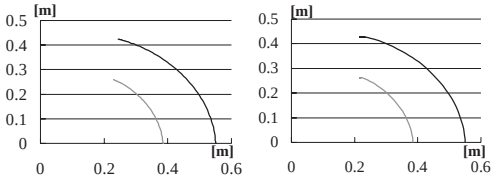

(a) (b)

Figure 7: *The experimental results. (a) A sequence of positions calculated by robot kinematics using angles measured by joint encoders. (b) A sequence of positions calculated by integrating accelerations twice captured from the acceleration scales.*

4.3. Initial Internal Force and Moment Measured by 6 DOF Force/Moment Sensor and High Speed Camera

After a stopping puck is pushed by a mullet, we obtain its final internal force/moment of the puck by summing all the external forces/moments acting on the puck. Firstly, we measure and summarize a sequence of internal forces and moments of a puck from its linear and angular accelerations measured by the scales (whose sampling time is 20 [μs]) via the Newton-Euler equations, and synchronously measure and summarize a sequence of external forces and moments between puck and mallet by the force/moment sensor (whose sampling time is 125 [μs]). After comparing two kinds of sequences with each other, we understand the former is better than the latter because of sampling time. For this reason, in our experiment, we obtain final linear/angular velocities by multiplying and summing all linear/angular accelerations and sampling time. Synchronously, we get linear/angular forces by Newton equation $\mathbf{F} = m\ddot{x}$ and Euler's equation $\mathbf{N} = \mathbf{J}\ddot{\theta}$, and then obtain final internal linear/angular forces by summing all the calculated linear/angular forces. Note that the m is measured by weight balance and inertia matrix $\mathbf{J}$ is calculated by density and volume of the puck.

- The internal force $\mathbf{F}_i$ and moment $\mathbf{N}_i$ of the puck can be calculated by the sum of forces/moments calculated from linear/angular accelerations under the Newton-Euler equations. The accelerations are measured by two acceleration scales per a given sampling time $\Delta t (= 20[\mu s])$.

$$\mathbf{F}(0) = \sum_{i=0}^{n} \mathbf{F}_i, \quad \mathbf{N}(0) = \sum_{i=0}^{n} \mathbf{N}_i \tag{12}$$

Therefore, we can identify initial internal force $\mathbf{F}(0)$ and moment $\mathbf{N}(0)$ of a puck which correspond to linear and angular velocities $\dot{x}(0)$ and $\dot{\theta}(0)$ before collision.

$$\dot{x}(0) = \sum_{i=0}^{n} \ddot{x}_i \Delta t \quad , \quad \mathbf{F}(0) = m \sum_{i=0}^{n} \ddot{x}_i \tag{13}$$

If $m = 0.008$ [kg] and $\Delta t = 0.00002$ [second] are substituted, we obtain the corresponding equation from an initial linear velocity to its internal force.

$$\mathbf{F}(0) = \frac{m\dot{x}(0)}{\Delta t} = 400\dot{x}(0) \tag{14}$$

$$\dot{\theta}(0) = \sum_{i=0}^{n} \ddot{\theta}_i \Delta t \quad , \quad \mathbf{N}(0) = \mathbf{J} \sum_{i=0}^{n} \ddot{\theta}_i \tag{15}$$

If $m = 0.008$ [kg] and $\Delta t = 0.00002$ [second], $r = 0.0324$ [m] are substituted, we obtain the corresponding equation from an initial angular velocity to its internal moment.

$$\mathbf{N}(0) = \mathbf{J}\frac{\dot{\theta}(0)}{\Delta t} = \frac{1}{2}\mathbf{m}r^2\frac{\dot{\theta}(0)}{\Delta t} = 0.20995\dot{\theta}(0) \qquad (16)$$

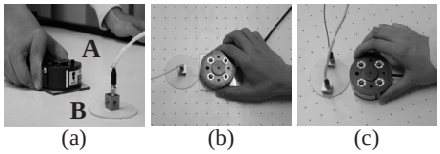

(a) (b) (c)

Figure 8: *The relation between acceleration and force, and that between angular acceleration and moment are synchronously measured by the acceleration scales and 6 DOF force/moment sensor. (a) A: 6 DOF force/moment sensor, B: acceleration scale. (b) measuring linear acceleration. (c) measuring angular acceleration.*

5. Comparative Results Between Mirtich's and Our Approaches

In this section, we firstly evaluate precision of linear and angular velocities before and after collision, which are measured by the high speed camera. Then, under experimental pairs of velocities before and after collision, we secondly evaluate our algorithm's superiority against Mitrich's algorithm concerning to accuracy of linear/angular impulses (linear/angular velocities after collision). In this experiment, we adopt an air hokey game that a human strikes a puck by a mallet. In our hokey table, the puck moves with constant linear/angular velocities because of no friction.

5.1. Identification of Momentum Variations (Impulse Areas) Before and After Collision

In our research, we use the color camera MotionScope PCI 1000sc (REDLAKE MASD Co.). The image resolutions are $480 \times 420 \sim 240 \times 210$, sampling time is 20 [ms] $\sim$ 1 [ms], and shatter speed is $1 \sim 20$ times smaller than the rate.

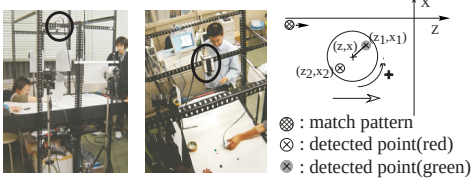

(a) (b) (c)

Figure 9: *(a),(b) A collision between two bodies is captured by the high speed camera, which are running in the air hockey table without any friction. (c) The position and orientation identification by color image processing based on two landmarks.*

The feature circles are colored as red and green. In order to identify each feature circle by its color, we normalize R,G,B as $r = R/(R+G+B)$, $g = G/(R+G+B)$, $b = B/(R+G+B)$. In our image processing, we are always seeking for each feature circle by color and size, and consequently calculate the center of gravity, e.g., (x_r, z_r) for red feature. If the number of feature circles is two, we use red and green for processing stability (Fig.9(c)). The X and Z coordinates x_c and y_c) of body center can be calculated by $x_c = (x_r + x_g)/2$ and $z_c = (z_r + z_g)/2$. In addition, the orientation of body is calculated as $arctan((x_r - x_g)/(z_r - z_g))$. After that, linear velocity of the body is calculated by dividing the distance of neighbor center points by 1 [ms]. Also, angular velocity of the body is calculated by dividing the difference between neighbor orientation angles by 1 [ms]. A puck is floating on a table, which is pushed by an air. Therefore, we need not consider any friction, and therefore we can see no linear and angular accelerations (Fig.10).

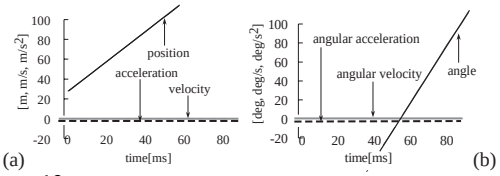

(a) (b)

Figure 10: *(a) Each moving object has constant velocity and has no acceleration. (b) Each has constant angular velocity and has no angular acceleration.*

5.2. Comparison Between Linear and Angular Velocities Measured by Acceleration Scales and High Speed Camera

As mentioned in the last paragraph, we measure linear/angular velocities of a puck by the high speed camera. Even though a puck moves a long distance, we can get its linear/angular velocities by this non-contact measurement. In this paragraph, we check precision of the velocities as follows: The sampling time (20 [μ s]) of the scale is fifty times smaller than that (1 [ms]) of the high speed camera. Therefore, the acceleration scale is better than the high speed camera to measure the velocities. Needless to say, since two scales on a pack are connected to PC by cables, the puck should move a short distance without considering their tensions.

By locating two scales on a puck (Fig.8), we firstly measure linear/angular accelerations and then linear/angular velocities by integrating the accelerations. Then, we compare the linear and angular velocities with corresponding velocities measured and calculated by the high speed camera. The maximum difference of linear velocities is bounded as $0.098[m/s]$, and the maximum difference of angular velocities is limited as $4.015[rad/s]$. These are small enough against linear and angular errors $0.205[m/s]$ and $12.352[rad/s]$ between Mirtich's and our approaches.

5.3. Comparative Results in Mirtich's and Our Approaches

In general, linear impulses p_x and p_z or angular impulse $p_{\theta y}$ correspond to linear momentum variations $m\Delta\dot{x}_x$ and $m\Delta\dot{x}_z$ or angular momentum variation $J\Delta\dot{\theta}_y$ theoretically. Also, linear momentum variations (e.g., $m\Delta\dot{x}_x$) are determined by variation between linear velocities (e.g., $\dot{x}_{bx}$ and $\dot{x}_{ax}$) before and after collision, and angular momentum variation $J\Delta\dot{\theta}_y$ is determined by variation between angular velocities $\dot{\theta}_{by}$ and $\dot{\theta}_{ay}$ before and after collision. For these reasons, if linear/angular velocities before collision are given, linear/angular velocities after collision can be controlled by linear and angular impulses (momentum variations) in dynamic animation.

First of all, we describe experimental results in ten trials. Table 1 illustrates a set of input data as linear/angular velocities and their internal force/moment before collision, i.e., $\dot{X}_{bx}$, $\dot{X}_{bz}$, $\dot{\Theta}_{by}$, F_x, F_z and N_y. As contrasted with this, Table 2 shows a set of output data as linear/angular velocities, i.e., $\dot{X}_{ax}$, $\dot{X}_{az}$ and $\dot{\Theta}_{ay}$ after collision, and linear/angular momentum variations $m\Delta\dot{x}_x$, $m\Delta\dot{x}_z$, $J\Delta\dot{\theta}_y$.

Secondly, we illustrate artificial results for the trials by Mitrich's and our approaches. Table 3 describes a set of Mirtich's output data as linear/angular velocities after collision, i.e., $\dot{x}_{ax}$, $\dot{x}_{az}$, $\dot{\theta}_{ay}$, and vertical/tangential impulses, i.e., p_x, p_z and $p_{\theta y}$. On the other hand, Table 4 shows a set of our output data as linear/angular velocities, i.e., $\dot{x}_{ax}$, $\dot{x}_{az}$, $\dot{\theta}_{ay}$, and vertical/tangential impulses after collision, i.e., p_x, p_z and $p_{\theta y}$.

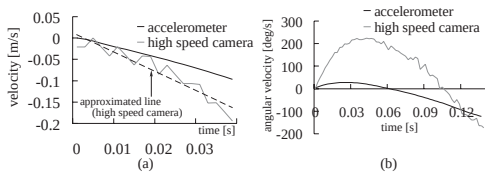

Figure 11: *(a) Linear velocities measured by the acceleration scales and the high speed camera. (b) Angular velocities measured by the acceleration scales and the high speed camera.*

As shown in these results, vertical linear velocity and impulse, tangential linear velocity and impulse, and angular velocity and impulse after collision in our approach are closer to experimental ones than those in Mirtich's approach. As a result, our impulse-based approach is better than Mirtich's one. Therefore, we ascertain the superiority of our approach considering balances between external/internal forces and moments under static/dynamic frictions during collision.

6. Conclusions and Future Works

In order to overcome drawbacks of Baraff's and Mirtich's force/impulsive force approaches, we propose a new precise approach to make linear and angular impulses exactly and artificially. In this approach, we can generate an artificial impulse that is really similar to its real impulse. Therefore, under our approach, a human can feel a real impulse (force distribution) during collision by some haptic and also can watch dynamic animation including simultaneous multiple contacts in a personal computer with a graphics accelerator. These applications should be realized in a near future.

References

1. D.Baraff, "Analytical Methods for Dynamic Simulation of Nonpenetrating Rigid Bodies," *Computer Graphics (Proc. of the SIGGRAPH)*, pp.223-232, July 1989.
2. D.Baraff, "Fast Contact Force Computation for Nonpenetrating Rigid Bodies." *Computer Graphics (Proc. of the SIGGRAPH)*, pp.23-34, July 1994.
3. B.V.Mirtich and J.F.Canny, "Impulse-based Dynamic Simulation", *The Workshop on the Algorithmic Foundations of Robotics*, In K.Goldberg, D.Halperin, J.C.Latombe, and R.Wilson, editors, A. K. Peters, pp.407-418, 1994.
4. B.V.Mirtich and J.F.Canny, "Impulse-Based Simulation of Rigid Bodies", *Proc. of the IEEE Int Symp. on Interactive 3D Graphics*, pp.181-188, 1995.
5. B.V.Mirtich, "Impulse-based Dynamic Simulation of Rigid Body Systems", *Ph.D Dissertation, University of California at Berkeley*, December 1996.
6. K.Kawachi, H.Suzuki and F.Kimura, "Simulation of Rigid Body Motion with Impulsive Friction Force," *Proc. of the IEEE International Symposium on Assembly and Task Planning*, pp.182-187, August 1997.
7. K.Kawachi, H.Suzuki and F.Kimura, "Technical Issues on Simulating Impulse and Friction in Three Dimensional Rigid Body Dynamics," *Proc. of the IEEE Computer Animation '98 Conference*, pp.170-176, June 1998.

Table 1: *Real collision between puck and wall: linear and angular velocities ($\dot{X}_b$ and $\dot{\Theta}_b$) before collision, and internal force and moment ($\mathbf{F}(0)$ and $\mathbf{N}(0)$) calibrated by the linear and angular velocities, respectively.*

trial	$\dot{X}_{bx}$ m/s	$\dot{X}_{bz}$ m/s	$\dot{\Theta}_{by}$ rad/s	F_x N	F_z N	N_y $N \cdot m$
1	0.909	-0.682	0.000	363.60	-272.80	0.0000
2	1.136	-1.136	40.221	830.87	-454.40	8.4444
3	1.364	-1.705	30.984	835.61	-682.00	6.5050
4	1.591	-1.818	0.000	636.40	-727.20	0.0000
5	2.045	-2.045	0.000	818.00	-818.00	0.0000
6	1.250	-2.273	-3.967	462.87	-909.20	-0.8329
7	1.932	-2.614	-7.126	706.10	-1045.60	-1.4961
8	1.705	-3.295	-6.347	622.59	-1318.00	-1.3326
9	1.364	-3.523	-5.105	497.81	-1409.20	-1.0719
10	3.295	-3.523	-6.687	1255.41	-1409.20	-1.4039

Table 2: *Real collision between puck and wall: linear and angular velocities ($\dot{X}_a$ and $\dot{\Theta}_a$) after collision, and linear and angular momentum variations ($m\Delta\dot{x}$ and $J\Delta\dot{\theta}$) calibrated by the linear and angular velocities, respectively*

trial	$\dot{X}_{ax}$ m/s	$\dot{X}_{az}$ m/s	$\dot{\Theta}_{ay}$ rad/s	$m\Delta\dot{x}_x$ kgm/s	$m\Delta\dot{x}_z$ kgm/s	$J\Delta\dot{\theta}_y$ kgm^2/s
1	0.682	0.455	8.236	-0.0018	0.0091	0.00004
2	1.136	0.682	36.138	0.0000	0.0145	-0.00001
3	1.136	1.250	43.485	-0.0018	0.0236	0.00005
4	1.364	1.250	11.186	-0.0018	0.0245	0.00005
5	1.705	1.136	10.772	-0.0027	0.0255	0.00005
6	1.023	1.250	7.121	-0.0018	0.0282	0.00005
7	1.705	1.477	7.111	-0.0018	0.0327	0.00006
8	1.364	1.818	19.838	-0.0027	0.0409	0.00011
9	0.909	1.932	15.346	-0.0036	0.0436	0.00009
10	2.841	1.932	16.039	-0.0036	0.0436	0.00010

Table 3: *Artificial collision between puck and wall: A set of linear and angular velocities ($\dot{x}$, $\dot{\theta}$) and impulse during collision, which is calculated in the Mirtich's approach.*

trial	$\dot{x}_{ax}$ m/s	$\dot{x}_{az}$ m/s	$\dot{\theta}_{ay}$ rad/s	p_x kgm/s	p_z kgm/s	$p_{\theta y}$ kgm^2/s
1	0.729	0.355	11.130	-0.0014	0.0083	0.00005
2	0.835	0.591	58.827	-0.0024	0.0138	0.00008
3	0.913	0.887	58.847	-0.0036	0.0207	0.00012
4	1.117	0.947	29.245	-0.0038	0.0221	0.00012
5	1.507	1.062	33.218	-0.0043	0.0249	0.00014
6	1.157	1.194	1.7850	-0.0007	0.0277	0.00002
7	1.577	1.366	14.798	-0.0028	0.0318	0.00009
8	1.650	1.732	-2.935	-0.0004	0.0402	0.00001
9	1.561	1.867	-17.282	0.0016	0.0431	-0.00005
10	2.380	1.832	49.786	-0.0073	0.0428	0.00024

Table 4: *Artificial collision between puck and wall: A set of linear and angular velocities ($\dot{x}$, $\dot{\theta}$) and impulse during collision, which is calculated in our new approach.*

trial	$\dot{x}_{ax}$ m/s	$\dot{x}_{az}$ m/s	$\dot{\theta}_{ay}$ rad/s	p_x kgm/s	p_z kgm/s	$p_{\theta y}$ kgm^2/s
1	0.804	0.391	4.671	-0.0008	0.0086	0.00002
2	0.952	0.652	48.431	-0.0015	0.0143	0.00003
3	1.088	0.979	43.306	-0.0022	0.0215	0.00005
4	1.317	1.043	12.194	-0.0021	0.0229	0.00005
5	1.735	1.174	13.810	-0.0025	0.0257	0.00006
6	0.882	1.305	12.423	-0.0029	0.0286	0.00007
7	1.509	1.500	11.740	-0.0034	0.0329	0.00008
8	1.172	1.891	17.421	-0.0043	0.0415	0.00010
9	0.794	2.022	20.295	-0.0046	0.0444	0.00011
10	2.725	2.022	18.714	-0.0046	0.0444	0.00011